

Neural Distributed Source Coding

Jay Whang*

jaywhang@cs.utexas.edu
University of Texas at Austin

Alliot Nagle*

acnagle@utexas.edu
University of Texas at Austin

Anish Acharya

anishacharya@utexas.edu
University of Texas at Austin

Hyeji Kim

hyeji.kim@austin.utexas.edu
University of Texas at Austin

Alexandros G. Dimakis

dimakis@austin.utexas.edu
University of Texas at Austin

July 18, 2023

Abstract

Distributed source coding (DSC) is the task of encoding an input in the absence of correlated side information that is only available to the decoder. Remarkably, Slepian and Wolf showed in 1973 that an encoder without access to the side information can asymptotically achieve the same compression rate as when the side information is available to it. While there is vast prior work on this topic, practical DSC has been limited to synthetic datasets and specific correlation structures. Here we present a framework for lossy DSC that is agnostic to the correlation structure and can scale to high dimensions. Rather than relying on hand-crafted source modeling, our method utilizes a conditional Vector-Quantized Variational AutoEncoder (VQ-VAE) to learn the distributed encoder and decoder. We evaluate our method on multiple datasets and show that our method can handle complex correlations and achieves state-of-the-art PSNR.

1 Introduction

Data compression plays an essential role in modern computer systems. From multimedia codecs running on consumer devices to cloud backups in large data centers, compression is a necessary component in any system that deals with high-volume or high-velocity sources. Applications such as multi-camera surveillance systems, IoT sensing, 3D scene capture and stereo imaging create distributed data streams with very large volume that are highly correlated.

We are interested in distributed compression – specifically the *distributed source coding* (DSC) problem. In this setting, there are two correlated sources (input x and side information y) that are physically separated. Both must be compressed and sent to a common decoder. We can assume that the side information y is compressed in isolation and communicated to the decoder and now one can expect that the original source x can be compressed at a higher-rate since y is known to the decoder.

The core challenge is how to compress the original source x when the correlated side information y is available only at the decoder as shown in Figure 1 (left). If side information is available to both the

encoder and decoder as in Figure 1 (right), it is well known that the side information can be utilized to improve the compression rate of x .

Surprisingly, Slepian and Wolf [1] showed that an encoder that has no access to the correlated side information can asymptotically achieve the same compression rate as when side information is available at both the encoder and the decoder.

In other words, *distributed* compression is asymptotically as efficient as *joint* compression. Later, Wyner and Ziv [2] extended this result to lossy compression. This is nothing short of a remarkable classical information theory result that defies intuition.

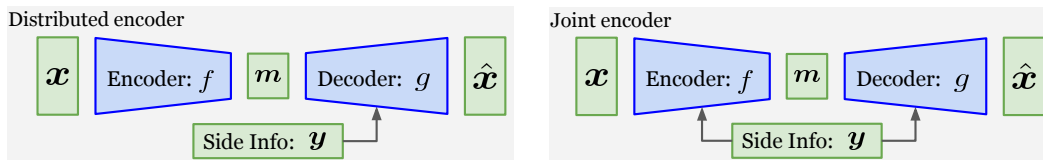


Figure 1: A distributed encoder that has no access to the correlated side-information (left) can asymptotically achieve the same compression rate as when side-information is available at both the encoder and the decoder (right).

1.1 Motivating Example

Here we present a simple example that highlights the intuition behind DSC. Let x and y be uniformly random 3-bit sources that differ by at most one bit. Clearly, losslessly compressing x requires 3 bits. However, if y is known to both encoder and decoder, then x can be transmitted using 2 bits instead. This is because the encoder can send the difference between x and y , which is uniform in $\{000, 001, 010, 100\}$. Thus, *joint* compression uses 2 bits.

Now, if the side information y is available only at the decoder, Slepian-Wolf theorem suggests that the encoder can still transmit x using only 2 bits. How could this be possible? The key idea is to group 8 possible values of x into 4 bins, each containing two bit-strings with maximal Hamming distance: $\mathcal{B}_0 = \{000, 111\}$, $\mathcal{B}_1 = \{001, 110\}$, $\mathcal{B}_2 = \{010, 101\}$, $\mathcal{B}_3 = \{011, 100\}$. Then the encoder simply transmits the bin index $m \in \{0, 1, 2, 3\}$ for the bin containing x . The decoder can produce the reconstruction \hat{x} based on the bin index m and y ; precisely, $\hat{x} = \arg \max_{x \in \mathcal{B}_m} P(x|y)$. Since x and y are off by at most one bit and the Hamming distance between the bit strings in each bin is 3, the decoder can recover x without error given y . In other words, the side information allows the decoder to correctly choose between the two candidates in the bin specified by the encoder. [3] advances this insight and introduces a constructive scheme for the distributed coding of correlated i.i.d. Bernoulli sources, denoted by Distributed Coding Using Syndromes (DISCUS).

This idea can be readily extended to *lossy* distributed compression by first quantizing the source, then applying Slepian-Wolf coding as was proposed by [2]. Several constructive schemes that combine the DISCUS along with quantization are proposed for correlated i.i.d. Gaussian sources and are shown to be near-optimal as the message length approaches infinity [3, 4].

1.2 Practical Difficulties

There are major challenges in designing practical distributed compression schemes for arbitrarily correlated sources. First, the joint distribution $p(x, y)$ is required to design the encoder and decoder, but modeling high-dimensional joint distributions (e.g. for correlated images) is very challenging, especially without modern deep generative models. Second, designing a distributed compression scheme with reasonable run time beyond simple structures remains an open question.

The significant gap between the theory and practice of DSC has been well-acknowledged in the information theory community. Two decades after the Slepian-Wolf theorem, [5] writes: “despite the existence of potential applications, the conceptual importance of Slepian–Wolf coding has not been mirrored in practical data compression.” Constructive compression schemes have been designed only for very special cases, such as correlated Bernoulli sources [3], Gaussian sources [4, 3], and stereo images (as elaborated in Section 2.3).

In this paper, we bridge this gap by leveraging the recent advances in deep generative modeling and show that it is possible to train an encoder and decoder for distributed compression of *arbitrarily* correlated high-dimensional sources. Specifically, our approach (denoted *Neural DSC*) parametrizes the encoder-decoder pair as a Vector-Quantized VAE (VQ-VAE) [6], so that: (a) we avoid needing a hand-crafted analytical model for the source distribution; (b) we can *learn* the complicated encoder and decoder mappings via neural networks with efficient inference; and (c) the discrete latent representation of VQ-VAE allows for a further rate improvement through post-hoc training of a latent prior (Section 3.2).

Our main contributions are as follows:

- We introduce Neural DSC, a compression scheme for lossy distributed source coding based on a particular type of VAE (VQ-VAE).
- We justify the use of VAE by establishing a connection between DSC and a modified evidence lower bound (ELBO) used to train VAEs for our asymmetric encoder-decoder setup.
- We show that Neural DSC performs favorably to existing techniques on stereo camera image compression, achieving state-of-the-art PSNR for all rates. Moreover, our method achieves competitive performance in MS-SSIM [7] even when compared to models specifically trained for it.
- We further validate that our approach can adapt to complex correlations and other modalities. We also provide concrete evidence that our method indeed performs DSC by comparing it to the theoretically optimal compressors on a synthetic dataset.

2 Background

2.1 ELBO & VAE

A variational auto-encoder (VAE) [8] is a special type of auto-encoder which regularizes the latent space such that the latent variable z is a Gaussian random variable. Typically, the training objective of auto-encoders is to minimize the reconstruction loss. However, the training objective of VAEs is motivated by learning the likelihood $p(\mathbf{x})$ of the training data, but instead of learning $p(\mathbf{x})$ directly, the VAE training objective seeks to maximize the evidence lower bound (ELBO). ELBO is a lower bound on the log-likelihood $p(\mathbf{x})$ of the training data, and it consists of a distortion (reconstruction) term and a rate term:

$$\log p(\mathbf{x}) \geq \text{ELBO}(\mathbf{x}) = \underbrace{\mathbb{E}_{q(z|\mathbf{x})} [\log p(\mathbf{x} | z)]}_{\text{distortion}} - \underbrace{D_{\text{KL}}(q(z | \mathbf{x}) \| p(z))}_{\text{rate}} \quad (1)$$

Intuitively, the distortion term represents the reconstruction loss, and the rate term regularizes the latent space such that the posterior $q(z | \mathbf{x})$ is close to the prior $p(z)$. It is often assumed that $p(z)$ is a zero mean isotropic Gaussian. As a special case, when $p(\mathbf{x} | z)$ is assumed to be Gaussian the distortion term becomes the ℓ_2 reconstruction loss. A derivation for ELBO is provided in [9], in addition to a detailed explanation of VAEs.

VAEs are commonly used for data compression; one such example is bits back coding [10]. Some earlier works [11, 12] have demonstrated the utility of VAEs for image compression, and these works form the backbone of recent works in the DSC setting [13, 14]; we discuss them in Section 2.3.

2.2 Vector-Quantized VAE

Vector-Quantized VAE (VQ-VAE) [6] is a specific type of VAE [8, 15] with a *discrete* latent variable, even when the input is continuous. Because the latent code is discrete and has fixed size, VQ-VAEs are a natural fit for lossy compression. Indeed, many existing works have explored its use in various compression tasks, ranging from music generation to high-resolution image synthesis [16–20].

A VQ-VAE consists of three components: an encoder, a decoder, and a codebook. The main difference between VQ-VAE and a regular VAE is that the output of the encoder is quantized to the nearest vector in the codebook. During training, all three components are jointly optimized. During inference, the input is represented by the index of the code vector that the encoder’s output is quantized to. Once a VQ-VAE is trained, it is common to use an autoregressive model, such as PixelCNN [21] or transformers [22], to achieve a lower rate for a fixed distortion value. The autoregressive model learns the joint distribution for the ordered set of latent codebook vectors used to represent each VQ-VAE input; this model can be used to lower the compression rate of the VQ-VAE via arithmetic coding [23].

2.3 Related Work

Unlike the vast literature that exists on distributed source coding (DSC), the use of deep learning on DSC has received relatively little attention. To the best of our knowledge, we are aware of two concurrent studies, which we describe below.

2.3.1 Distributed Stereo Image Compression

[24] proposes a method to perform DSC for stereo camera image pairs with a high spatial correlation. Due to the large spatial similarity between the images, one of them can serve as the side information for the other. The key component of their method is the “Side Information Finder”, a module that finds similar image patches between the side information and the reconstructed signal produced by a pre-trained autoencoder. Since the two images have many approximately overlapping patches, the reconstruction is further improved by copying over matching image patches from the side information to the reconstruction.

While this leads to a considerable improvement in compression performance, this method is only applicable when the input and side information have large spatial overlap. On the other hand, our method is applicable to any correlated sources. We empirically validate this using data sources with substantially more complex correlation (see Figure 8).

2.3.2 Neural Distributed Image Compression

[13] leverages a (regular) VAE for DSC of image data; the proposed architecture is designed to explicitly model the common information between the input and side information. Intuitively, the goal is to guide the encoder to compress only the portion that is not recoverable from the side information. Once trained, the encoder simply discards the common information and only transmits the residual, with the hope of decoder being able to reconstruct the common information from the side information. [14] further adapt this architecture by encoding and decoding the side information in parallel to the input image decoder network and utilizing cross attention modules between the two decoder networks. They report that the cross attention modules allow for better alignment between the latent representations of the side information and the input image, thereby enabling better utilization of the side information.

3 Neural Distributed Source Coding

In this section, we derive our ELBO bound for the DSC setting. We discuss the connection of our distributed ELBO bound to the optimization objective of NDIC-CAM [14], the state-of-the-art baseline we compare our work to. We use our distributed ELBO bound to motivate a new loss for the VQ-VAE architecture.

3.1 ELBO and Distributed Source Coding

VAEs have been extensively used for neural compression [11, 25, 12], as its training objective, ELBO, can be interpreted as a sum of rate and distortion of a lossy compressor as shown in Equation (1). For example when the decoder $p(\mathbf{x} | \mathbf{z})$ is Gaussian, the first term turns into the widely-used ℓ_2 distortion.

However, this interpretation breaks down in our asymmetric encoder-decoder setup where only the decoder has access to the side information \mathbf{y} . In this setup, we are interested in modelling the conditional likelihood $p(\mathbf{x} | \mathbf{y})$ as opposed to the likelihood $p(\mathbf{x})$ for the symmetric (vanilla VAE) case. We can show that the corresponding objective in our setup, which we call *distributed ELBO* (or dELBO for short), is in fact a lower bound to the conditional log-likelihood $\log p(\mathbf{x} | \mathbf{y})$:

Proposition 1. *Let $\mathbf{x}, \mathbf{y}, \mathbf{z}$ be random variables following the conditional independence structure $\mathbf{y} \rightarrow \mathbf{x} \leftarrow \mathbf{z}$. Then for any choice of posterior $q(\mathbf{z} | \mathbf{x})$ valid under p (i.e. $\text{supp } q(\mathbf{z} | \mathbf{x}) \subseteq \text{supp } p(\mathbf{z})$ for all \mathbf{x}), we have*

$$\log p(\mathbf{x} | \mathbf{y}) \geq \mathbb{E}_q [\log p(\mathbf{x} | \mathbf{y}, \mathbf{z})] - D_{\text{KL}}(q(\mathbf{z} | \mathbf{x}) \| p(\mathbf{z})) \triangleq \text{dELBO}(\mathbf{x}, \mathbf{y}).$$

Proof:

$$\begin{aligned} \log p(\mathbf{x} | \mathbf{y}) &= \mathbb{E}_{\mathbf{z} \sim q(\cdot | \mathbf{x})} [\log p(\mathbf{x} | \mathbf{y})] \\ &= \mathbb{E}_q [\log p(\mathbf{x}, \mathbf{y}, \mathbf{z}) - \log p(\mathbf{z} | \mathbf{x}, \mathbf{y}) - \log p(\mathbf{y})] \\ &= \mathbb{E}_q [(\log p(\mathbf{x}, \mathbf{y} | \mathbf{z}) + \log p(\mathbf{z})) + (\log q(\mathbf{z} | \mathbf{x}) - \log q(\mathbf{z} | \mathbf{x}))] \\ &\quad - \mathbb{E}_q [\log p(\mathbf{z} | \mathbf{x}, \mathbf{y}) - \log p(\mathbf{y})] \\ &= \mathbb{E}_q [-(\log q(\mathbf{z} | \mathbf{x}) - \log p(\mathbf{z})) + (\log q(\mathbf{z} | \mathbf{x}) - \log p(\mathbf{z} | \mathbf{x}, \mathbf{y}))] \\ &\quad + \mathbb{E}_q [\log p(\mathbf{x}, \mathbf{y} | \mathbf{z}) - \log p(\mathbf{y})] \\ &= -D_{\text{KL}}(q(\mathbf{z} | \mathbf{x}) \| p(\mathbf{z})) + D_{\text{KL}}(q(\mathbf{z} | \mathbf{x}) \| p(\mathbf{z} | \mathbf{x}, \mathbf{y})) \\ &\quad + \mathbb{E}_q [\log p(\mathbf{x}, \mathbf{y} | \mathbf{z}) - \log p(\mathbf{y})] \\ &\geq -D_{\text{KL}}(q(\mathbf{z} | \mathbf{x}) \| p(\mathbf{z})) + \mathbb{E}_q [\log p(\mathbf{x}, \mathbf{y} | \mathbf{z}) - \log p(\mathbf{y})] \\ &\stackrel{A}{=} -D_{\text{KL}}(q(\mathbf{z} | \mathbf{x}) \| p(\mathbf{z})) + \mathbb{E}_q [\log p(\mathbf{x} | \mathbf{y}, \mathbf{z}) + \log p(\mathbf{y} | \mathbf{z}) - \log p(\mathbf{y})] \\ &= -D_{\text{KL}}(q(\mathbf{z} | \mathbf{x}) \| p(\mathbf{z})) + \mathbb{E}_q [\log p(\mathbf{x} | \mathbf{y}, \mathbf{z})] = \text{dELBO}(\mathbf{x}, \mathbf{y}) \end{aligned}$$

where (A) follows from our assumption that \mathbf{y} and \mathbf{z} are marginally independent. Negating both side of the inequality completes the proof. Note that the dELBO rate term, $D_{\text{KL}}(q(\mathbf{z} | \mathbf{x}) \| p(\mathbf{z}))$, matches the rate term in ELBO. Intuitively, this makes sense since the rate is controlled by the encoder, which does not have access to the side information \mathbf{y} . The DSC setting provides the decoder with access to correlated side information \mathbf{y} , and that is reflected in the dELBO distortion term.

The importance of this connection between ELBO and distributed source coding is two fold. First, it shows that there is a tractable surrogate objective that minimizes the optimal conditional compression rate $-\log p(\mathbf{x} | \mathbf{y})$, which is also the asymptotically optimal rate for distributed coders [1, 2]. Second, and perhaps more importantly, this scheme also allows us to obtain a practically useful encoder-decoder pair whose rate-distortion we can control as we shall see later.

Finally, we point out that dELBO is a special case of the loss objective proposed in Equation 1 of the NDIC-CAM work [14]. Beyond the dELBO terms, their loss objective includes terms for the

rate and distortion of the side information \mathbf{y} , controlled by hyperparameter α , and the rate of their proposed *common information*, controlled by hyperparameter β . Note that their objective is dELBO when $\alpha = \beta = 0$, and they empirically show that this case yields the best performance.

3.2 Our Method

3.2.1 Notation and Setup

We let \mathbf{x} , \mathbf{y} , and \mathbf{m} to denote the original message, correlated side information, and compressed message, respectively. The *encoder* f maps the given message to a low-dimensional vector $f(\mathbf{x})$, which is then quantized to the closest code vector:

$$c_{\mathbf{m}} = \arg \min_{c \in \mathcal{C}} \|c - f(\mathbf{x})\|,$$

where the table of code vectors \mathcal{C} is jointly trained with the encoder f and the decoder g . We then transmit the index \mathbf{m} of the quantized vector losslessly. The *decoder* g in turn tries to reconstruct the input signal using the compressed message and side info: $\hat{\mathbf{x}} = g(c_{\mathbf{m}}; \mathbf{y})$. Note that the encoder only receives \mathbf{x} , while the decoder receives both \mathbf{m} and the side information \mathbf{y} .

We refer to the number of bits required to transmit \mathbf{m} as the *rate*, and the reconstruction performance (measured by ℓ_2 error or MS-SSIM) as the *distortion*.

3.2.2 Training Objective

We train the distributed encoder-decoder pair (f, g) along with the codebook \mathcal{C} as a conditional VQ-VAE, where only g is conditioned on the side information \mathbf{y} .

$$\mathcal{L}(f, g, \mathcal{C}) = \|g(c_{\mathbf{m}}; \mathbf{y}) - \mathbf{x}\|^2 + \beta \|f(\mathbf{x}) - \text{stop_grad}(e_{\mathbf{m}})\|^2. \quad (2)$$

This loss can be interpreted as a weighted sum of log-likelihood under Gaussian decoder (distortion) and a vector quantization term that tries to bring encoder output close to existing code vectors, which in turn has an impact on the resulting rate. This training objective is derived from dELBO in a similar-fashion as the original VQ-VAE objective was derived from ELBO [6]. Namely, we assume that $p(\mathbf{z})$ is uniform and $D_{\text{KL}}(q(\mathbf{z} | \mathbf{x}) \| p(\mathbf{z}))$ is therefore constant with respect to the encoder parameters and can be removed from the objective, we add the commitment loss (the second term in Equation (2)), and codebook \mathcal{C} is jointly updated as an exponential moving average of code vectors following the original VQ-VAE work.

The network is trained on i.i.d. pairs $(\mathbf{x}^{(i)}, \mathbf{y}^{(i)})$ to minimize the desired distortion between the input \mathbf{x} and the reconstruction $\hat{\mathbf{x}}$. This scheme allows us to directly train the encoder-decoder pair in an end-to-end manner without needing to model or manually specify the correlation structure between \mathbf{x} and \mathbf{y} .

3.2.3 Why VQ-VAE?

Although much of the existing literature has focused on VAEs as the backbone for neural compression [11, 26, 12, 25, 27], we intentionally chose VQ-VAE instead for a few reasons. First, VQ-VAE offers an explicit control over the rate through the latent dimension and codebook size – unlike VAEs for which we can only estimate the rate after training the model. VQ-VAE also guarantees an upper bound on the resulting rate regardless of the input, which is often desired in practice (e.g. communication channel with strict maximum bandwidth limit). Finally, a rate improvement can be achieved for a trained VQ-VAE by fitting a latent prior model to the VQ-VAE’s discrete latent space; we demonstrate such a rate improvement in Figure 2a. The downside of using a VQ-VAE is that training is less stable than a VAE, but this did not pose much issue during our experiments.

3.2.4 Use of a Latent Prior

Our VQ-VAE architecture achieves comparable performance to other methods in the DSC setting. However, the aggregate posterior learned by VQ-VAE is often far from uniform in practice. This allows for a further rate improvement by losslessly compressing the latent codes by fitting a discrete prior over them. Following [6], we use an autoregressive prior based on Transformer [22], which can be readily used with arithmetic coding [23] to obtain a lossless compressor that closely matches the model’s negative log-likelihood.

Specifically, we use the decoder-only Transformer trained with maximum-likelihood objective on discrete latent codes. This differs from the original VQ-VAE work [6], which utilized a PixelCNN prior. Transformer has been shown to achieve better performance compared to PixelCNN variants [28, 17]. We provide VQ-VAE results with (solid blue line) and without (dashed blue line) the latent prior, as shown in Figure 2. When we use the latent prior, we are able to outperform all other methods on PSNR, and match the best method on MS-SSIM.

4 Experiments

We demonstrate the efficacy of our framework through a diverse set of experiments. In our stereo image compression experiments, we match or exceed the performance of all baselines. Then, we methodically investigate how well VQ-VAEs handle complex correlations between the input message and side information in the distributed, joint, and separate cases. Finally, we provide a proof of concept experiment to show how our framework can be used in distributed training.

4.1 Stereo Image Compression

4.1.1 Setup

We first evaluate our method on stereo image compression. Following [24], we construct a dataset consisting of pairs of images obtained from the KITTI Stereo 2012 and 2015 [29, 30]. Each pair of images are taken by two cameras at a slightly different angle and share spatial similarity (see Figure 8, left). The goal is to compress one of the images in each pair, treating the other image as side information that only the decoder has access to. The performance of a compressor is evaluated by its rate-distortion points, where rate and distortion are measured in terms of bits/pixel (bpp) and Peak Signal-to-Noise Ratio (PSNR).

For each target rate, we train a conditional VQ-VAE as described in Section 3.2. We then evaluate its distortion averaged over the test set, and plot the rate-distortion point. The exact details of how the dataset is constructed as well as the model hyperparameters are included in the Appendix.

4.1.2 Results

We compare our methods to existing distributed image compression methods DSIN [24] and NDIC [13]. As shown in Figure 2a, our method achieves new state-of-the-art PSNR at all rate regions.

In Figure 2b, we see that our model remains competitive compared to NDIC-CAM [14], which currently achieves the best results for MS-SSIM. We point out that all our models were trained on PSNR, so explicitly training the VQ-VAEs to maximize MS-SSIM will likely further improve their performance on this benchmark.

In addition, our model is significantly more parameter-efficient compared to [13]. Table 1 shows the parameter count for the models used to generate the points in Figure 2a. As shown, our models are smaller by a factor of up to $\sim 6\times$.

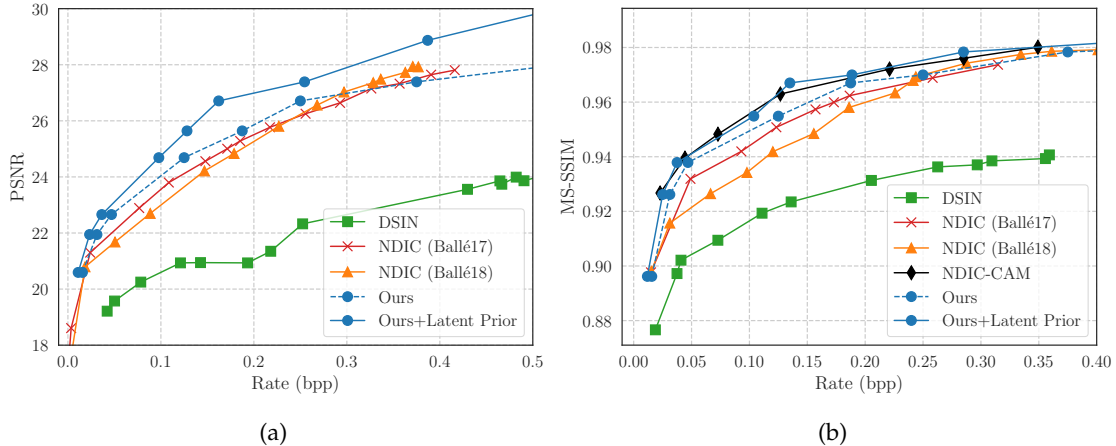


Figure 2: **(a)** PSNR rate-distortion curves on the KITTI Stereo image dataset. Our method achieves higher PSNR than other methods for low rates and remains competitive for higher rates. With the latent prior model, we outperform all methods. **(b)** Comparison of MS-SSIM rate-distortion curves on the KITTI Stereo image dataset. Despite only training on PSNR loss, our approach remains competitive for higher rates.

Table 1: Number of model parameters for the rate-distortion points (both VQ-VAE and latent prior model) in Figure 2a.

	Parameter Count (M)	Factor
Ours	3.9 – 7.4	1.0-1.9×
NDIC (Ballé17)	16.3	4.2×
NDIC (Ballé18)	25.0	6.4×

4.2 Handling Complex Correlation

4.2.1 Setup

To further investigate how well our method can handle complex correlation between the input and side information, we evaluate our method on a challenging distributed compression setup. First we create a dataset of correlated images from 256×256 CelebA-HQ dataset [31] containing images of celebrity faces. Each image is vertically split into top and bottom halves, where the top half is used as the input and the bottom half is used as side information (see Figure 8, right). Following [32], we use 27000/3000 split between train/test data.

While there is clearly some correlation between the top and bottom halves of an image of a human face, modeling this correlation (e.g. the conditional distribution over the top half of a face given the bottom half) is highly nontrivial. This experiment is thus designed to show our model’s ability to leverage this correlation to improve compression.

4.2.2 Baseline VQ-VAEs

To analyze the gains from distributed compression, we train three different variants of VQ-VAEs: distributed (our method), joint, and separate. In the *joint* model, both the encoder and decoder have access to the side information. This serves as a proxy to the intractable theoretical rate-distortion bound established by [2] for lossy distributed compression. We expect this to be the upper limit on the

performance of our method. The *separate* model is positioned at the other extreme, where neither the encoder nor the decoder uses the side information. This serves as the lower limit on the performance of our method. To ensure a fair comparison among these variants, they have identical architecture and number of parameters for the autoencoder portion, and only vary in the way they handle the side information. Architectural details and network hyperparameters are provided in the Appendix.

4.2.3 Results

In Figure 3, we see that the distributed VQ-VAE achieves nearly identical performance as the joint VQ-VAE, further proving the viability of our method as a distributed coding scheme.

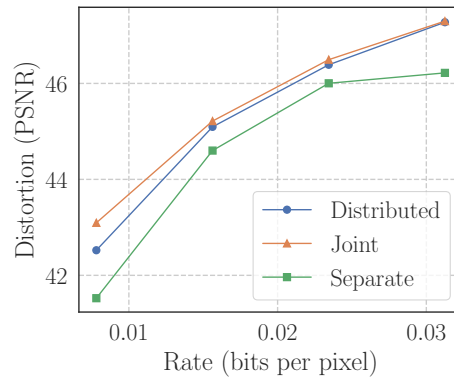


Figure 3: Comparison of different coding schemes on CelebA-HQ. This shows that the distributed encoder is able to nearly match the performance of joint encoder, while achieving a noticeable improvement in rate-distortion over the “separate” encoder that does not utilize side information.

4.2.4 Effect of Side Information

It is possible that the distributed VQ-VAE learns to ignore the side information, effectively collapsing to a separate VQ-VAE. We investigate whether the distributed decoder actually makes use of the side information by intentionally providing incorrect input.

We show in Figure 4 that the side information plays a significant role in the quality of reconstruction. For example, providing a side information with a different face leads to the reconstruction having a matching skin tone that is different from the original. As expected, side information has no effect for the separate encoder.



Figure 4: Reconstructions from distributed encoder under different side information. We can see that providing wrong or random side information to the distributed decoder affects the output in a semantic way (e.g. the skin tone changes, while the background remains identical).

4.3 Communication Constrained Distributed Optimization

4.3.1 Background

Here we consider an interesting proof of concept that applies our method to distributed training of a neural network h_θ with parameters $\theta \in \mathbb{R}^d$. With the increasing size of deep learning models, an important bottleneck in distributed training is the repeated communication of gradients between workers and the parameter server. To alleviate this issue, many gradient compression techniques have been developed.

A key observation we make is that the gradients coming from different workers are correlated. This suggests that individual workers may be able to compress their gradients via distributed source coding without having to communicate with each other. We compare this approach to a representative subset of baselines, which we describe in Appendix A.1.6. While our approach is not ready for a practical deployment, we observe a vastly improved training performance, suggesting a promising direction for future research.

4.3.2 Experimental Setup

We focus on a simple setup where two workers $j = 1, 2$ are assigned a subset $\mathcal{X}_j \in \mathcal{X}$ of the training data. The workers then compute gradients locally using SGD-like iterations and communicate the gradients back to a central parameter server. At each iteration t , the correlation between the client gradients \mathbf{g}_t^1 and \mathbf{g}_t^2 can be exploited to further improve compression performance. Concretely, we treat \mathbf{g}_t^1 as side information and train a distributed encoder for \mathbf{g}_t^2 , and show that the cost of communicating \mathbf{g}_t^2 can be substantially reduced.

The neural network h_θ being trained using compressed gradients is a small convolutional network for MNIST digit classification [33]. We partition the MNIST training data \mathcal{X} into two equal subsets: \mathcal{X}_{pre} and \mathcal{X}_{train} . \mathcal{X}_{pre} is used to train the VQ-VAE encoder and \mathcal{X}_{train} is used to train h_θ using the trained encoder as gradient compressor. We measure the performance of our method using two metrics: (a) **rate-distortion** of the distributed compressor, and (b) **classification accuracy** of the model h_θ trained using compressed gradients.

4.3.3 Generating training data for encoder

We train h_θ for T steps using the Adam optimizer across two nodes over \mathcal{X}_{pre} . This generates a sequence of T gradient pairs $\{\mathbf{g}_t^1, \mathbf{g}_t^2\}_{t=1}^T$, which can be used to train the VQ-VAE encoders.

However, naively applying our method to this setting leads to a suboptimal VQ-VAE as these gradient pairs are highly correlated across training steps. Noticing that \mathbf{g}_t^1 and \mathbf{g}_t^2 are conditionally independent given the initial model weights and the time step t , we train h_θ for multiple runs with different initialization for θ , while randomly sampling a subset of gradients from each run. Thus we generate a dataset of tuples $(t, \mathbf{g}_t^1, \mathbf{g}_t^2)$ sampled from multiple independent runs. We also update the architecture of the VQ-VAE so that both the encoder and decoder are conditioned on t . This way, the gradients become i.i.d. samples over random runs and time steps.

4.3.4 Pre-training VQ-VAE encoders

We first compare the performance of three different VQ-VAE variants over the course of a single training run of h_θ . As shown in Figure 5a, we observe a substantial improvement in ℓ_2 distortion for the distributed VQ-VAE, compared to the separate model. As training progresses, the gap between the joint and distributed encoders narrows, suggesting that a sufficiently large distributed VQ-VAE encoder can nearly match the performance of its joint counterpart.

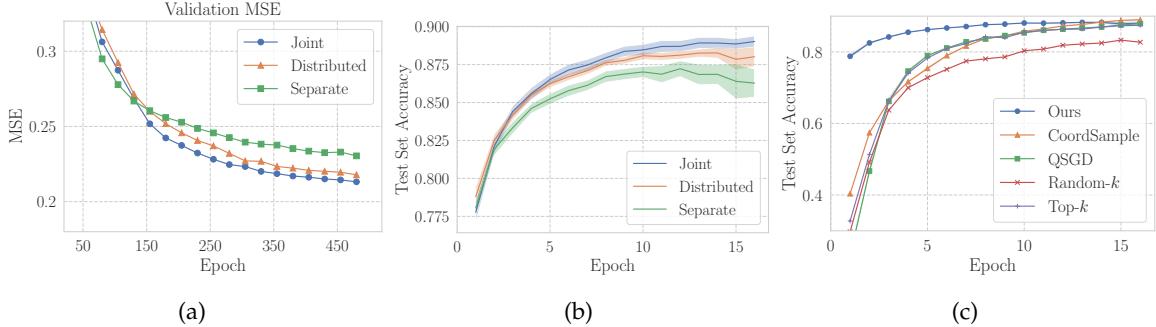


Figure 5: **(a)** Average ℓ_2 distortion over the validation split during the course of VQ-VAE training. We observe that the distributed encoder significantly outperforms the separate encoder and approaches the distortion of the joint encoder. **(b)** Plot of the average test set accuracy over the course of training h_θ using compressed gradients. We observe that the distributed encoder leads to comparable accuracy as the joint encoder, but using about only half of the communication cost. Shaded regions represent standard error. **(c)** Distributed training performance with compressed gradients using a distributed encoder in comparison to other baseline methods in terms of test set accuracy. Note that standard error is very small and barely visible, and may require zooming in on an electronic copy of this manuscript.

4.3.5 Distributed Training

Given the pre-trained encoders, we train h_θ using gradients compressed by the pre-trained encoder. We compare it against the baseline gradient compression schemes listed above: Top- k , Rand- k , QSGD and Coordinated Sampling. All runs were repeated 20 times with different random seeds, and we report average performance along with standard error.

Figure 5b shows that h_θ trained with gradients compressed using the distributed VQ-VAE leads to substantial accuracy improvement over the separate VQ-VAE without the extra communication cost. Moreover, we see that VQ-VAE based compression leads to about $3\times$ faster convergence than the baselines (see Figure 5c). This shows that a learned distributed encoder can indeed benefit from the complex correlation between gradients distributed optimization.

5 Discussion and Analysis

In this section, we further provide discussion and analysis on our framework. Namely, we first analyze the effect of reconstruction diversity as we vary side information. Next, we perform a sanity check to see whether our approach is indeed performing DSC by comparing with the optimal distributed compressor. Finally, we compare the performance of our approach with DISCUS [3] in a setting with simpler correlation structure between the source and side information.

5.1 Role of Side Information

In Section 1.1 we saw that grouping symbols with maximal distance from each other in the same group allows the decoder to determine the correct symbol using the side information. Here we investigate to what extent our models perform such a grouping (also known as *binning*). If approximate binning was occurring, the same codeword (i.e. bin index) would be decoded into different images for different side information. In other words, a distributed compressor should have high reconstruction diversity for a single codeword as we vary the side information. We refer to this as *bin diversity*.

On the other hand, a model that does not perform binning should decode a single codeword to similar symbols regardless of what side information is given to the decoder. To test this hypothesis, we

train two different models: **Ours** was trained with the correct side information as was done for other experiments; and **Uncorrelated SI** was trained by replacing the side information with random ones from other, irrelevant samples in the dataset, thus making the input and side information completely independent. We expect this model to ignore side information and achieve lower bin diversity.

To quantitatively measure diversity, we used average pairwise distance with respect to ℓ_2 norm and LPIPS distance [34], which has been used in the literature [35, 36] as a measure of sample diversity. Both metrics were computed and averaged over all images in the CelebA-HQ test dataset.

As shown in Table 2, the VQ-VAE trained with correlated side information exhibits much higher bin diversity in both metrics. In other words, the images within each bin are much farther from each other compared to the other model, suggesting that some form of approximate binning is happening. The uncorrelated VQ-VAE has particularly low bin diversity with respect to the LPIPS distance, meaning there is very little perceptual difference regardless of what side information is used.

Table 2: Diversity of decoded samples as we vary side information.

	Diversity (LPIPS)	Diversity (ℓ_2)
Ours	0.1130	35.80
Uncorrelated SI	0.00469	4.167

5.2 Optimality of the Learned Compressor.

Another natural question to ask is how close our *learned* distributed compressor is to the optimal distributed compressor. We investigate this using a synthetic data source studied in [3] with two correlated Gaussian sources: $Y = X + N$, $X \sim \mathcal{N}(0, 1)$, and $N \sim \mathcal{N}(0, 0.1^2)$. The asymptotically optimal (i.e. in the limit of compressing infinitely many symbols together) rate-distortion curve of these sources is known analytically, so we can check how our model compares to the theoretical limit.

Figure 6a shows that for low rates, both learned methods significantly outperform the asymptotically optimal encoder without side information (SI). This is a concrete evidence that our learned encoder is actually performing DSC (as opposed to simply achieving a very good compression rate for single source coding) Moreover, the distributed compression performance remains very close to that of joint compression, showing the efficacy of our practical distributed coding scheme.

At higher rates, however, the value of side information quickly diminishes, and the learned methods perform worse than even the encoder without SI. This is expected as the optimal curves presented in this figure are asymptotic in the limit of jointly compressing infinitely many symbols, which is clearly not the case for the learned methods that compress each symbol one at a time.

5.3 Comparison with Non-learning Baselines

5.3.1 Setup

We consider a simple but systematic correlation structure: correlated i.i.d. Bernoulli sources [3]. Specifically, we consider a pair of source sequence and side information $(\mathbf{x}, \mathbf{y}) = \{x_i, y_i\}_{i=1}^{648}$, where $y_i \oplus x_i$ is an i.i.d. Bernoulli random variable.

We compare the performance of our Neural DSC approach¹ with the Distributed Source Coding Using Syndromes (DISCUS), a non-learning based constructive scheme that is designed specifically

¹Implementation details are provided in Appendix A.1.7.

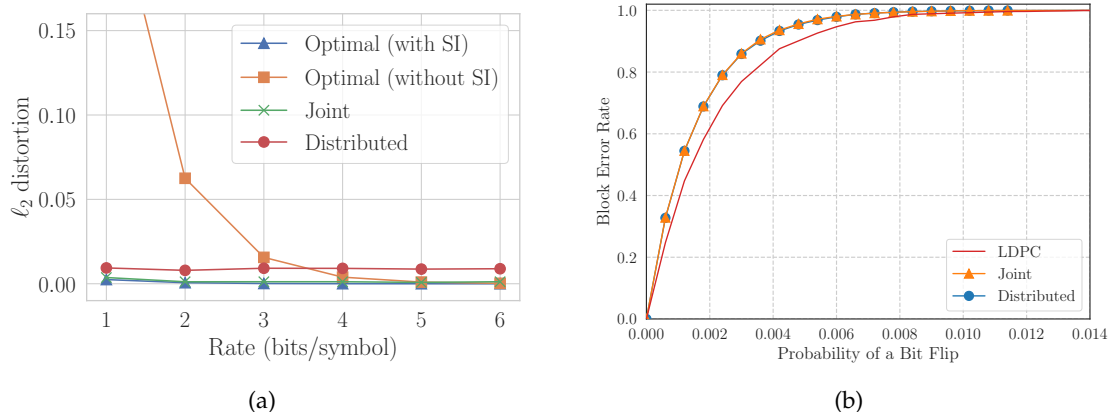


Figure 6: **(a)** Rate-distortion points of learned joint and distributed encoders compared to theoretically best compressors. The “Optimal” curves represent the asymptotically optimal rate-distortion points and are included as reference. Note that these are theoretical limits and do not correspond to any concrete compression scheme. **(b)** Block error rate for our VQ-VAE architecture and an LDPC implementation of DISCUS on i.i.d. Bernoulli messages.

for this setup and shown to be near optimal [3].² Our experimental results are shown in Figure 6b. As expected, our neural DSC performs worse than DISCUS (labeled as LDPC); however, the performance of distributed neural DSC is comparable with the performance of joint source coding, which serves as a sanity check.

5.3.2 Interpretation

Unlike other experiments, here we focus on a systematic correlation structure, where the problem at hand is learning a complex *algorithm*; there is no complexity in the data structure. These results show that even in such scenarios, our method learns a nontrivial compression algorithm (i.e., a compression scheme without side information achieves the block error rate ≈ 1).

6 Conclusion

We presented Neural DSC, a framework for distributed compression of correlated sources. Our method is built on the power of modern deep generative models, namely VQ-VAEs, which are excellent data-driven models to represent high-dimensional distributions using compressed discrete latent codes. Our training objective is justified in part by the connection we establish between distributed source coding and the modified ELBO for asymmetric VAEs.

Empirically, we show that our method achieves the new state-of-the-art performance in terms of PSNR on stereo image compression. Our approach remains competitive with current best results for MS-SSIM. We also show that our method is able to leverage complex correlations far beyond spatial similarity for better compression performance, approaching the joint compression rate. Finally, we show that our method is not limited to images and show a promising proof of concept for compressing gradients for distributed training. We believe that our work provides encouraging initial results for practical data-driven DSC and hope to see further developments.

²For the formulation of the syndrome in the DISCUS algorithm, we use a quasi-cyclic LDPC code that is adopted in the communication standards. Details for the LDPC’s construction are provided in Appendix A.1.8.

Acknowledgments

This research has been supported by NSF Grants CCF 1934932, AF 1901292, 2008710, 2019844 the NSF IFML 2019844 award as well as research gifts by Western Digital, WNCG and MLL, computing resources from TACC and the Archie Straiton Fellowship.

References

- [1] D. Slepian and J. Wolf. Noiseless coding of correlated information sources. *IEEE Transactions on Information Theory*, 19(4):471–480, 1973. doi: 10.1109/TIT.1973.1055037.
- [2] A. Wyner and J. Ziv. The rate-distortion function for source coding with side information at the decoder. *IEEE Transactions on Information Theory*, 22(1):1–10, 1976. doi: 10.1109/TIT.1976.1055508.
- [3] S.S. Pradhan and K. Ramchandran. Distributed source coding using syndromes (discus): design and construction. In *Proceedings DCC'99 Data Compression Conference (Cat. No. PR00096)*, pages 158–167, 1999. doi: 10.1109/DCC.1999.755665.
- [4] Yang Yang, S. Cheng, Zixiang Xiong, and Wei Zhao. Wyner-ziv coding based on tcq and ldpc codes. In *The Thirty-Seventh Asilomar Conference on Signals, Systems & Computers, 2003*, volume 1, pages 825–829 Vol.1, 2003. doi: 10.1109/ACSSC.2003.1292028.
- [5] S. Verdu. Fifty years of shannon theory. *IEEE Transactions on Information Theory*, 44(6):2057–2078, 1998. doi: 10.1109/18.720531.
- [6] Aaron van den Oord, Oriol Vinyals, and Koray Kavukcuoglu. Neural discrete representation learning. In *Proceedings of the 31st International Conference on Neural Information Processing Systems*, pages 6309–6318, 2017.
- [7] Zhou Wang, Eero P Simoncelli, and Alan C Bovik. Multiscale structural similarity for image quality assessment. In *The Thrity-Seventh Asilomar Conference on Signals, Systems & Computers, 2003*, volume 2, pages 1398–1402. Ieee, 2003.
- [8] Diederik P. Kingma and Max Welling. Auto-encoding variational bayes. In Yoshua Bengio and Yann LeCun, editors, *2nd International Conference on Learning Representations, ICLR 2014, Banff, AB, Canada, April 14-16, 2014, Conference Track Proceedings, 2014*. URL <http://arxiv.org/abs/1312.6114>.
- [9] Diederik P. Kingma and Max Welling. An introduction to variational autoencoders. *Foundations and Trends® in Machine Learning*, 12(4):307–392, 2019. ISSN 1935-8237. doi: 10.1561/22000000056. URL <http://dx.doi.org/10.1561/22000000056>.
- [10] James Townsend, Thomas Bird, and David Barber. Practical lossless compression with latent variables using bits back coding. In *International Conference on Learning Representations, 2019*. URL <https://openreview.net/forum?id=ryE98iR5tm>.
- [11] Johannes Ballé, Valero Laparra, and Eero P. Simoncelli. End-to-end optimized image compression, 2017.
- [12] Johannes Ballé, David Minnen, Saurabh Singh, Sung Jin Hwang, and Nick Johnston. Variational image compression with a scale hyperprior. In *6th International Conference on Learning Representations, ICLR 2018, Vancouver, BC, Canada, April 30 - May 3, 2018, Conference Track Proceedings. OpenReview.net, 2018*. URL <https://openreview.net/forum?id=rkcQFMZRb>.
- [13] Nitish Mital, Ezgi Ozyilkan, Ali Garjani, and Deniz Gunduz. Neural distributed image compression using common information, 2021.

- [14] Nitish Mital, Ezgi Özyilkan, Ali Garjani, and Deniz Gündüz. Neural distributed image compression with cross-attention feature alignment. In *Proceedings of the IEEE/CVF Winter Conference on Applications of Computer Vision (WACV)*, pages 2498–2507, January 2023.
- [15] Danilo Jimenez Rezende, Shakir Mohamed, and Daan Wierstra. Stochastic backpropagation and approximate inference in deep generative models. In *International conference on machine learning*, pages 1278–1286. PMLR, 2014.
- [16] Cristina Garbacea, Aaron van den Oord, Yazhe Li, Felicia S C Lim, Alejandro Luebs, Oriol Vinyals, and Thomas C Walters. Low bit-rate speech coding with vq-vae and a wavenet decoder. *ICASSP 2019 - 2019 IEEE International Conference on Acoustics, Speech and Signal Processing (ICASSP)*, May 2019. doi: 10.1109/icassp.2019.8683277. URL <http://dx.doi.org/10.1109/ICASSP.2019.8683277>.
- [17] Ali Razavi, Aaron van den Oord, and Oriol Vinyals. Generating diverse high-fidelity images with vq-vae-2. In H. Wallach, H. Larochelle, A. Beygelzimer, F. d'Alché-Buc, E. Fox, and R. Garnett, editors, *Advances in Neural Information Processing Systems*, volume 32. Curran Associates, Inc., 2019. URL <https://proceedings.neurips.cc/paper/2019/file/5f8e2fa1718d1bbcfd9c7a54fb8c-Paper.pdf>.
- [18] Adam Roberts, Jesse Engel, Colin Raffel, Curtis Hawthorne, and Douglas Eck. A hierarchical latent vector model for learning long-term structure in music. In *International Conference on Machine Learning*, pages 4364–4373. PMLR, 2018.
- [19] Aditya Ramesh, Mikhail Pavlov, Gabriel Goh, Scott Gray, Chelsea Voss, Alec Radford, Mark Chen, and Ilya Sutskever. Zero-shot text-to-image generation. *arXiv preprint arXiv:2102.12092*, 2021.
- [20] Jiahui Yu, Yuanzhong Xu, Jing Yu Koh, Thang Luong, Gunjan Baid, Zirui Wang, Vijay Vasudevan, Alexander Ku, Yinfei Yang, Burcu Karagol Ayan, et al. Scaling autoregressive models for content-rich text-to-image generation. *arXiv preprint arXiv:2206.10789*, 2022.
- [21] Aäron van den Oord, Nal Kalchbrenner, Oriol Vinyals, Lasse Espeholt, Alex Graves, and Koray Kavukcuoglu. Conditional image generation with pixelcnn decoders. In *Proceedings of the 30th International Conference on Neural Information Processing Systems, NIPS'16*, page 4797–4805, Red Hook, NY, USA, 2016. Curran Associates Inc. ISBN 9781510838819.
- [22] Ashish Vaswani, Noam Shazeer, Niki Parmar, Jakob Uszkoreit, Llion Jones, Aidan N. Gomez, Łukasz Kaiser, and Illia Polosukhin. Attention is all you need. In *Proceedings of the 31st International Conference on Neural Information Processing Systems, NIPS'17*, page 6000–6010, Red Hook, NY, USA, 2017. Curran Associates Inc. ISBN 9781510860964.
- [23] Glen G Langdon. An introduction to arithmetic coding. *IBM Journal of Research and Development*, 28(2):135–149, 1984.
- [24] Sharon Ayzik and Shai Avidan. Deep image compression using decoder side information. In *Computer Vision - ECCV 2020 - 16th European Conference, Glasgow, UK, August 23-28, 2020, Proceedings, Part XVII*, volume 12362, pages 699–714, 2020.
- [25] David Minnen, Johannes Ballé, and George Toderici. Joint autoregressive and hierarchical priors for learned image compression. In *Proceedings of the 32nd International Conference on Neural Information Processing Systems*, pages 10794–10803, 2018.
- [26] Lucas Theis, Wenzhe Shi, Andrew Cunningham, and Ferenc Huszár. Lossy image compression with compressive autoencoders, 2017.

- [27] Johannes Ballé, Philip A. Chou, David Minnen, Saurabh Singh, Nick Johnston, Eirikur Agustsson, Sung Jin Hwang, and George Toderici. Nonlinear transform coding. *IEEE Trans. on Special Topics in Signal Processing*, 15, 2021. URL <https://arxiv.org/pdf/2007.03034>.
- [28] XI Chen, Nikhil Mishra, Mostafa Rohaninejad, and Pieter Abbeel. PixelSNAIL: An improved autoregressive generative model. In Jennifer Dy and Andreas Krause, editors, *Proceedings of the 35th International Conference on Machine Learning*, volume 80 of *Proceedings of Machine Learning Research*, pages 864–872. PMLR, 10–15 Jul 2018. URL <https://proceedings.mlr.press/v80/chen18h.html>.
- [29] Andreas Geiger, Philip Lenz, and Raquel Urtasun. Are we ready for autonomous driving? the kitti vision benchmark suite. In *2012 IEEE conference on computer vision and pattern recognition*, pages 3354–3361. IEEE, 2012.
- [30] Moritz Menze, Christian Heipke, and Andreas Geiger. Joint 3d estimation of vehicles and scene flow. *ISPRS annals of the photogrammetry, remote sensing and spatial information sciences*, 2:427, 2015.
- [31] Ziwei Liu, Ping Luo, Xiaogang Wang, and Xiaoou Tang. Deep learning face attributes in the wild. In *Proceedings of the IEEE international conference on computer vision*, pages 3730–3738, 2015.
- [32] Durk P Kingma and Prafulla Dhariwal. Glow: Generative flow with invertible 1x1 convolutions. In *Neural Information Processing Systems*, pages 10215–10224, 2018.
- [33] Yann LeCun, Corinna Cortes, and CJ Burges. Mnist handwritten digit database. *ATT Labs [Online]*. Available: <http://yann.lecun.com/exdb/mnist>, 2, 2010.
- [34] Richard Zhang, Phillip Isola, Alexei A Efros, Eli Shechtman, and Oliver Wang. The unreasonable effectiveness of deep features as a perceptual metric. In *Proceedings of the IEEE conference on computer vision and pattern recognition*, pages 586–595, 2018.
- [35] Akash Srivastava, Lazar Valkov, Chris Russell, Michael U Gutmann, and Charles Sutton. Veegan: Reducing mode collapse in gans using implicit variational learning. In *Proceedings of the 31st International Conference on Neural Information Processing Systems*, pages 3310–3320, 2017.
- [36] Luke Metz, Ben Poole, David Pfau, and Jascha Sohl-Dickstein. Unrolled generative adversarial networks. *arXiv preprint arXiv:1611.02163*, 2016.
- [37] Hongyi Wang, Scott Sievert, Shengchao Liu, Zachary Charles, Dimitris Papailiopoulos, and Stephen Wright. Atomo: Communication-efficient learning via atomic sparsification. In *Advances in Neural Information Processing Systems*, pages 9850–9861, 2018.
- [38] Anastasia Koloskova, Tao Lin, Sebastian U Stich, and Martin Jaggi. Decentralized deep learning with arbitrary communication compression. *arXiv preprint arXiv:1907.09356*, 2019.
- [39] Shaohuai Shi, Xiaowen Chu, Ka Chun Cheung, and Simon See. Understanding top-k sparsification in distributed deep learning. *arXiv preprint arXiv:1911.08772*, 2019.
- [40] Sebastian U Stich, Jean-Baptiste Cordonnier, and Martin Jaggi. Sparsified SGD with memory. In *Advances in Neural Information Processing Systems*, pages 4447–4458, 2018.
- [41] Dan Alistarh, Demjan Grubic, Jerry Li, Ryota Tomioka, and Milan Vojnovic. QSGD: Communication-efficient SGD via gradient quantization and encoding. In *Advances in Neural Information Processing Systems*, pages 1709–1720, 2017.
- [42] Debraj Basu, Deepesh Data, Can Karakus, and Suhas Diggavi. Qsparse-local-SGD: Distributed SGD with quantization, sparsification and local computations. In *Advances in Neural Information Processing Systems*, pages 14668–14679, 2019.

- [43] Shaohuai Shi, Qiang Wang, Kaiyong Zhao, Zhenheng Tang, Yuxin Wang, Xiang Huang, and Xiaowen Chu. A distributed synchronous sgd algorithm with global top-k sparsification for low bandwidth networks. In *2019 IEEE 39th International Conference on Distributed Computing Systems (ICDCS)*, pages 2238–2247. IEEE, 2019.
- [44] IEEEStandards. IEEE draft standard for information technology – telecommunications and information exchange between systems local and metropolitan area networks – specific requirements - part 11: Wireless LAN medium access control (MAC) and physical layer (PHY) specifications. *IEEE P802.11-REVmd/D1.0, February 2018*, pages 1–4226, 2018.
- [45] MATLAB. LDPC encoding and LDPC QuasiCyclicMatrix. <https://www.mathworks.com/help/comm/ref/ldpcencode.html>, 2021. Accessed: 01-25-2023.

A Appendix

A.1 Experiment Details

A.1.1 VQ-VAE Architecture

For our image compression experiments, we used a convolutional VQ-VAE architecture similar to the one used in [19] with residual connections.

Both the input and the side information to this network have the shape 128×256 (i.e. vertical halves of a full 256×256 image). The encoder scales down input image by a factor of $4\times$ or $8\times$ both vertically and horizontally, producing latent variables of shape 32×64 and 16×32 , respectively. Each dimension of the latent variable is allotted different numbers of bits (i.e. codebook bits), which range from 1 to 8 in our experiments. The decoder conversely takes a discrete latent variable and upscales it by a factor of $4\times$ or $8\times$ to produce a reconstruction of the original shape.

A detailed specification of the architecture is provided in Figure 7. The notation $(T\text{conv})$ “Conv $A \times B$ ($C \rightarrow D$)” represents a 2D (transposed) convolution with kernel size A and stride B with input and output channels C and D , respectively. The boxes “Residual Block ($A \rightarrow B$)” represent a two-layer residual network. We used GELU (Gaussian Error Linear Unit) activation for all layers except for the very last convolution of the decoder, for which we used sigmoid. The exact number of channels may differ for different rate-distortion points, and we refer the reader to the supplementary code submission for full details.

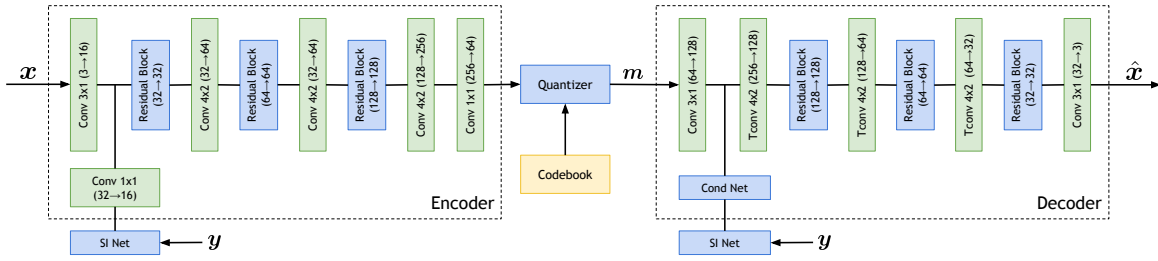


Figure 7: Conditional VQ-VAE architecture used for the image compression experiments.

We used a small network (denoted “SI Net”) shared by the encoder and decoder to preprocess the side information. Whenever the encoder or decoder does not receive side information (for distributed and separate VQ-VAEs), we simply replace the output of SI Net with a zero tensor of the same shape.

We note that all three VQ-VAE variants have the same architecture and number of parameters for the autoencoder portion (the portion that the horizontal line goes through in Figure 7). Thus there is no architectural advantage among the VQ-VAE variants.

A.1.2 Specifying Target Rate

The shape and the number of codebook bits determine the total rate. This is different from neural compression models that use a regular VAE, which control rate-distortion by reweighting the training objective (ELBO). As mentioned in Section 3.2, the fact that we have a hard constraint on the rate is useful when working with a hard communication limit.

There are several ways to achieve a desired target rate. For example, an $8\times$ downscaling encoder with 4 codebook bits produces compressed message of size $16 \times 32 \times 4 = 2048$ bits. The same rate can be achieved using a $4\times$ downscaling encoder with 1 codebook bit: $32 \times 64 \times 1 = 2048$ bits. This flexibility is what allows us to have a fairly granular control over the target rate, at the cost of hyperparameter choices.

Hyperparameters for KITTI Stereo Experiment. Due to the above choices, we use differently sized networks for each rate-distortion curve for our stereo image compression experiments. While the model definition is included in the code, we include the relevant hyperparameter information in Table 3 below.

Table 3: Different models and their associated hyperparameters for the stereo image compression experiment. Each row represents a single rate-distortion point in Figure 2a.

Downscaling Factor	Codebook Size (bits)	Rate (bpp)	PSNR	MS-SSIM	Parameter count
8×	1	0.0156	20.77	0.867	3,954,853
8×	2	0.0312	21.884	0.902	3,955,111
8×	3	0.0469	22.658	0.917	6,250,747
8×	8	0.125	24.687	0.945	4,037,827
4×	3	0.1875	25.642	0.959	6,276,619
4×	4	0.2500	26.582	0.969	6,277,651
4×	6	0.3750	27.531	0.973	6,283,843
2×	3	0.75	28.870	0.976	2,463,883
2×	4	1.0	30.101	0.983	2,464,915

Hyperparameters for CelebA-HQ Experiment. For this experiment, we used the single 8× downscaling encoder with codebook bits {1, 2, 3, 4}, resulting in the total rates of {512, 1024, 1536, 2048}.

Distributed optimization. For gradient compression VQ-VAEs, we followed the same architecture as the image compression experiments, but replaced all convolutional layers with fully-connected layers. Full specification of the network is included in the code submission.

A.1.3 Stereo Image Dataset

For our stereo image compression experiment, we follow the setup of [13]. First, we construct training/test datasets using the files specified in the official repository for [24] (https://github.com/ayzikhsha/DSIN/tree/master/src/data_paths). Then we apply the same preprocessing steps of [13], where we first take the center crop of size 370 × 740, then resizing it to 128 × 256 using PyTorch transformations. This results in the training split containing 1576 pairs of stereo images and test split containing 790 pairs.



Figure 8: (Left) Sample image pair from the KITTI Stereo dataset [29] used for the stereo image compression experiment. (Right) Image pairs used to test the model’s ability to handle complex correlations beyond spatial similarities. This was obtained by vertically splitting CelebA-HQ [31] images.

A.1.4 Training Details

For stereo image compression experiments, we trained our models for up to 1000 epochs on a DGX machine. Some training runs were early stopped because the validation performance started to plateau. For CelebA-HQ experiments, we trained the VQ-VAEs for a total of 20 epochs distributed over two

Nvidia GTX 2080 GPUs. For gradient compression experiments, we trained the fully-connected VQ-VAEs for 500 epochs on a single GPU.

In all cases, we evaluated validation loss after each epoch and observed no overfitting. This leads us to believe that it may be possible to further improve the performance of our method by training a larger network, which we leave for future work.

The latent prior models were implemented as an autoregressive transformer decoder network. All latent prior models were trained with an initial learning rate of $3e-4$ with a cosine annealing learning rate decay. Training lasted 100 epochs and the learning rate had a linear warmup period for the first 2000 steps of training. The ADAM optimizer was used with parameters $\beta_1 = 0.9$, $\beta_2 = 0.999$, $\epsilon = 1e-8$. The hyperparameters for each latent prior model are provided in Table 4. The models were trained on an RTX 3090 GPU, and due to memory constraints some of the latent prior models had to be trained with fewer blocks, fewer attention heads, and a smaller batch size than some of the other models.

Table 4: Different VQ-VAE models and the associated hyperparameters for their latent prior model counterparts for the stereo image compression experiment. Each row represents a single rate-distortion point in Figure 2a.

Downscaling Factor	Codebook Size (bits)	Rate (bpp) with Latent Prior	# Attn Heads Per Block	# Blocks	Batch Size	Parameter count
8×	1	0.0110	4	4	128	859,394
8×	2	0.0233	4	4	128	859,908
8×	3	0.0364	4	4	128	860,936
8×	8	0.0978	4	4	128	924,672
4×	3	0.1281	4	4	16	1,057,544
4×	4	0.1622	4	4	16	1,059,600
4×	6	0.2545	4	4	16	1,071,936
2×	3	0.3869	2	2	5	1,447,432
2×	4	0.5395	2	2	5	1,449,488

A.1.5 NDIC Training Details

For the CelebA-HQ compression experiment, we trained NDIC [13] using the official code released by the authors. We used the “Balle18” [12] backbone and trained the model for 10 epochs ($\approx 300K$ examples). For evaluation, we used the model checkpoint with the best validation set performance. While [13] report training with a batch size of 1 for 500K steps, we chose to use a batch size of 20. This was done for several reasons. First, using a batch size of 1 is very inefficient as we do not benefit from parallelism of GPU. It also leads to high variance in the gradient, often leading to slower convergence. In our training, the loss plateaued well before reaching 300K total examples. We also used MSE instead of MS-SSIM as the objective, since our models were also trained using MSE loss. This ensures a fair comparison in both training as well as evaluation, as we report PSNR (which is equivalent to MSE). The rest of the model hyperparameters were not modified.

A.1.6 Distributed Training Baselines

Here we list the baseline techniques used for gradient compression:

- **Random- k** [37, 38]: Instead of communicating the full gradient vector $\mathbf{g} \in \mathbb{R}^d$, we only transmit randomly chosen k coordinates, thus reducing the communication cost by a factor of $\frac{k}{d}$.
- **Top- k** [39, 40]: Similar to Random- k , this approach also communicates k of the d coordinates of a gradient vector and improves the communication cost by a factor of $\frac{k}{d}$. However, this time we take

the top k coordinates with largest magnitude and discard the remaining $(d - k)$ coordinates.

- **QSGD** [41, 42]: Gradients normally stored using 32-bit floating point numbers are quantized using fewer bits before being transmitted.
- **Coordinated Sampling** [43]: The nodes *cyclically* select a batch of k coordinates at every iteration and communicate only those k coordinates.

A.1.7 Neural DSC Training Details for i.i.d. Bernoulli experiments

A schematic of the VQ-VAEs trained in the joint and distributed settings is shown in Figure 9. A primary difference between this architecture and the architecture for the other experiments is that the output of the decoder of this architecture has a learnable parameter α which is used to linearly interpolate the reconstructed sequence and the side information, i.e., the output of the network is $(1 - \alpha)\hat{x} + \alpha y$, where \hat{x} is the reconstruction and y is the side information. This enables the VQ-VAE architecture to find a tradeoff between the reconstruction and the side information as the final reconstruction of the Bernoulli sequence. Our VQ-VAE architectures were trained on i.i.d. Bernoulli sequences of length 648, and the block error rate was computed on a fixed validation set of 10,000 i.i.d. Bernoulli sequences. All models were trained with the same hyperparameters: 128 batch size, $3e-4$ learning rate, 0.15 commitment cost (for the VQ-VAE loss), 10 epochs. The Adam optimizer was used with parameters $\beta_1 = 0.9$, $\beta_2 = 0.999$, $\epsilon = 1e - 8$.

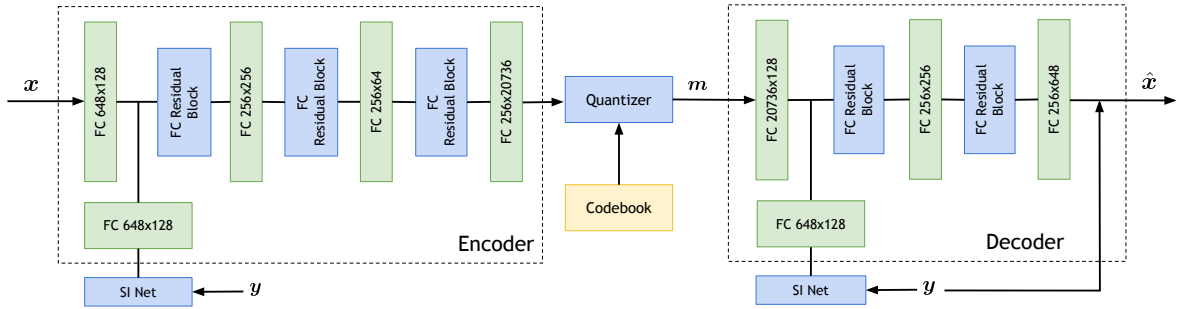


Figure 9: Conditional VQ-VAE architecture used for the DISCUS experiments.

A.1.8 DISCUS Details

For the experiment on the correlated i.i.d. Bernoulli sources (Figure 6b), we implemented the DISCUS [3] using a rate 3/4 Low-Density Parity Check (LDPC) code, specified in IEEE 802.11 [44], [45], which maps 486 message bits to a length-648 codeword. The parity-check matrix is created using the `ldpcQuasiCyclicMatrix` function, with the block size 27 and prototype matrix P defined as

$$P^T = \begin{bmatrix} 16 & 25 & 25 & 9 & 24 & 2 \\ 17 & 12 & 18 & 7 & 5 & 2 \\ 22 & 12 & 26 & 0 & 26 & 19 \\ 24 & 3 & 16 & 1 & 7 & 14 \\ 9 & 3 & 22 & 17 & 1 & 24 \\ 3 & 26 & 23 & -1 & -1 & 1 \\ 14 & 6 & 9 & -1 & -1 & 15 \\ -1 & 21 & -1 & 7 & 15 & 19 \\ 4 & -1 & 0 & 3 & 24 & -1 \\ 2 & 15 & -1 & -1 & 15 & 21 \\ 7 & 22 & 4 & 3 & -1 & -1 \\ -1 & -1 & -1 & 23 & 8 & 2 \\ 26 & 15 & 4 & -1 & -1 & -1 \\ -1 & -1 & -1 & 16 & 13 & 24 \\ 2 & 4 & 8 & -1 & -1 & -1 \\ -1 & -1 & 23 & -1 & 13 & 3 \\ 21 & -1 & 11 & 21 & -1 & -1 \\ -1 & 16 & -1 & -1 & 11 & 2 \\ 1 & -1 & -1 & 0 & -1 & 1 \\ 0 & 0 & -1 & -1 & -1 & -1 \\ -1 & 0 & 0 & -1 & -1 & -1 \\ -1 & -1 & 0 & 0 & -1 & -1 \\ -1 & -1 & -1 & 0 & 0 & -1 \\ -1 & -1 & -1 & -1 & 0 & 0 \end{bmatrix}.$$